

Depth Completion with Multiple Balanced Bases and Confidence for Dense Monocular SLAM

Weijian Xie*, Guanyi Chu*, Quanhao Qian*, Yihao Yu, Hai Li, Danpeng Chen, Shangjin Zhai, Nan Wang, Hujun Bao, Guofeng Zhang†

Abstract—Dense SLAM based on monocular cameras does indeed have immense application value in the field of AR/VR, especially when it is performed on a mobile device. In this paper, we propose a novel method that integrates a light-weight depth completion network into a sparse SLAM system using a multi-basis depth representation, so that dense mapping can be performed online even on a mobile phone. Specifically, we present a specifically optimized multi-basis depth completion network, called BBC-Net, tailored to the characteristics of traditional sparse SLAM systems. BBC-Net can predict multiple balanced bases and a confidence map from a monocular image with sparse points generated by off-the-shelf keypoint-based SLAM systems. The final depth is a linear combination of predicted depth bases that can be optimized by tuning the corresponding weights. To seamlessly incorporate the weights into traditional SLAM optimization and ensure efficiency and robustness, we design a set of depth weight factors, which makes our network a versatile plug-in module, facilitating easy integration into various existing sparse SLAM systems and significantly enhancing global depth consistency through bundle adjustment. To verify the portability of our method, we integrate BBC-Net into two representative SLAM systems. The experimental results on various datasets show that the proposed method achieves better performance in monocular dense mapping than the state-of-the-art methods. We provide an online demo running on a mobile phone, which verifies the efficiency and mapping quality of the proposed method in real-world scenarios.

Index Terms—Depth Completion, Dense SLAM, Multi-Basis

I. INTRODUCTION

REAL-TIME 6-DoF pose estimation and reconstruction of the surrounding environment is a fundamental problem for AR/VR. Existing monocular visual (-inertial) odometry or SLAM methods [1]–[5] based on multi-view geometry already achieved great success in pose estimation. However, these methods can only generate sparse point clouds or semi-dense maps, which have difficulties in handling complex AR applications such as collision detection and occlusion handling. While dense SLAM methods [6]–[9] can be used to generate real-time dense meshes, they often require additional sensors such as Time-of-Flight (ToF), LiDAR, etc. Considering the economic cost, a more ideal approach is to generate dense

H. Bao and G. Zhang, H. Li are with the State Key Lab of CAD&CG, Zhejiang University. E-mails: {baohujun, zhangguofeng, garyli}@zju.edu.cn.

W. Xie and D. Chen are with the State Key Lab of CAD&CG, Zhejiang University and SenseTime Research. D. Chen is also affiliated with Tetras.AI. E-mails: xieweijian@sensetime.com, chendanpeng@tetras.ai.

G. Chu, Q. Qian, Y. Yu, S. Zhai and N. Wang are with SenseTime Research. N. Wang is also affiliated with Tetras.AI. E-mails: {chuguanyi1, qianquanhao1, yuyihao, zhaishangjin}@sensetime.com, wangnan@tetras.ai.

* Equal contribution

† Corresponding author

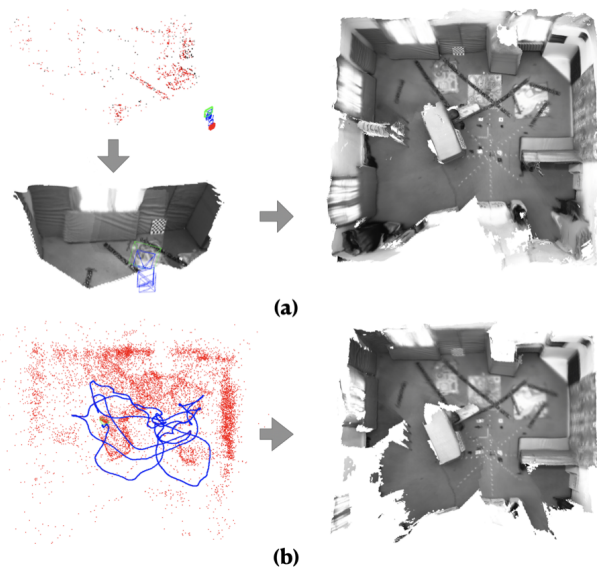


Fig. 1. (a) The real-time dense mapping process of BBC-ORBSLAM. BBC-Net complements the sparse depth generated by traditional sparse SLAM (left top of (a)) to dense depth (left bottom of (a)). By incorporating the predicted depth into SLAM optimization, a globally consistent mesh is obtained (right of (a)). (b) The dense mapping result of BBC-VINS. Our method can also recover a globally consistent dense mesh (right of (b)) from point clouds with poor quality generated by VINS (left of (b)).

meshes using a monocular camera, which remains a highly challenging problem, especially on resource-constrained mobile devices.

With the development of deep learning, many end-to-end methods [10]–[15] have emerged to address dense mapping or semi-dense mapping from a monocular camera. However, these methods often require significant computational resources, making them unsuitable for mobile devices. Traditional sparse SLAM methods remain the mainstream solution for real-time pose estimation due to their efficiency in practical applications. Recently, depth prediction from a single image [16], [17] and depth completion [18]–[29] from sparse depth inputs has emerged. A straightforward idea is to couple the depth prediction results into a traditional monocular SLAM framework.

Some methods [30]–[33] have been proposed to utilize the depth predicted by the network to improve the accuracy of SLAM. However, these methods will no longer optimize the depth once generated or just align the scale of the predicted depth, which makes the global consistency of the depth cannot be maintained. GeoRefine [34] incorporates RAFT-flow [35]

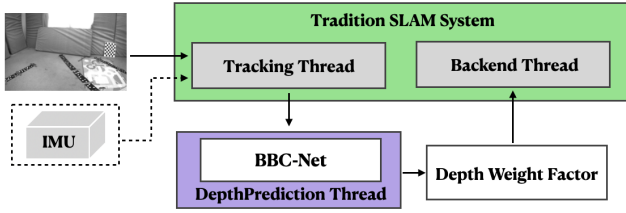


Fig. 2. General framework. When integrating our method into a traditional SLAM system, it is as simple as passing the sparse depths generated by the tracking module to BBC-Net and then incorporating the predicted bases and confidence, represented as depth weight factors, into the SLAM’s optimizer.

to enhance the front-end tracking and utilizes self-supervised learning to improve depth accuracy, making it evidently a non-lightweight solution. Methods in [36]–[38] use a variational autoencoder to compress dense depth into low-dimensional codes, which can be integrated into the optimization process of traditional SLAM to optimize dense depth. However, based on their experimental results, these methods demonstrate limited effectiveness in improving SLAM trajectory accuracy. Moreover, a critical limitation of these methods is their heavy reliance on GPU-based computations. It is not only during the calculation of the Jacobian matrix that GPU is required but also after each optimization iteration to infer new dense depths using GPU. In this work, we propose a highly flexible framework (as shown in Figure 2) to seamlessly transform a traditional sparse SLAM into a dense SLAM. With minimal modifications to the existing sparse SLAM, our method can efficiently achieve this conversion without introducing significant additional computational burden. Similar to CodeVIO [37], CodeMapping [38], we incorporate the network-predicted depth into the optimization of traditional SLAM to achieve global consistent depths. The difference is that we employ a multi-basis depth representation, which avoids redundant network inferences, making our method much more efficient and well-suited for mobile applications.

Qu et al. [21] propose a single-frame depth completion network with multi-scale depth representation. However, it only addressed the scenario of single-frame depth completion. Integrating the depth completion results into a SLAM system will bring new and more complex challenges. Firstly, the imbalance between the depth bases predicted by [21] and the imbalance introduced by continuously optimizing sparse points are not conducive to the fusion with a continuously optimizing SLAM system. Second, the quality of the depth predicted by the network is difficult to control, and it is crucial to prevent poor-quality depth predictions from adversely affecting the optimization results. To address these issues, we present BBC-Net, which predicts the multiple balanced bases and confidence from a monocular image and sparse points. The final depth is the linear combination of predicted balanced bases. BBC-Net is specifically optimized for sparse SLAM systems, allowing it to adapt to the noise in sparse points and the need for continuous optimization. To the best of our knowledge, we are the first to integrate multi-basis depth representation with traditional SLAM systems. The main contributions of this paper are listed as follows:

- We propose a light-weight multi-basis depth completion network, named BBC-Net, which is specifically designed for achieving dense monocular SLAM, by addressing the issue of imbalance in bases and predicting balanced bases with confidence simultaneously.
- In order to efficiently incorporate the weights of depth bases into the traditional optimizer while ensuring robustness, we design a set of weight factors with a marginalization scheme. When coupling with different SLAM systems, we can combine these factors to achieve a balance between speed and accuracy based on specific requirements.
- We propose a complete framework to integrate the proposed BBC-Net as a plugin into traditional sparse monocular SLAM systems, thus transforming them into dense SLAM systems. To illustrate the transformation from sparse SLAM to dense SLAM, we have chosen two representative sparse SLAM systems, ORB-SLAM3 [1] and VINS system (introduced in Sec. V-A), as exemplary cases to showcase our integration framework.
- We develop an online demo that runs on a mobile phone, which verifies the efficiency of our method and demonstrates the mapping quality in real-world scenarios.

The experiments on various datasets demonstrate that our method achieves better performance than the state-of-the-art in monocular dense mapping. Figure 1 shows an example.

II. RELATED WORK

A. Depth Completion

Single-frame depth recovery [16], [17] is challenging to ensure the global consistency of depth and is easily disturbed by an optical illusion. Since many sparse map points are generated in the process of SLAM tracking, depth completion based on these points can ensure global consistency while not bringing too much system burden as a multi-frame depth prediction net. Existing depth completion methods can be cataloged as early fusion, late fusion, and iterative approaches. Ma et al. [18] propose a ResNet-based model to take early fusion data that combines the RGB image and sparse depth points as single input. Methods like [18]–[20] show that early fusion performs well with the uniformly distributed sparse depth. Qu et al. [21] employ multi-scale bases as the network output instead of directly outputting the final depth. Then, they use a least squares module to calculate the weights of the depth bases and obtain the final depth. This creative design allows the net to work well with very sparse depths. Late fusion methods [22]–[24], [26] utilize different encoder networks to extract features from RGB images and depth, and then concatenate the extracted features to predict the depth. Some iterative fusion methods [25], [27]–[29] predict affinities from the initial depths, and iterative updates the initial depth using the learned affinities, which is unsuitable for very sparse depth.

B. VIO/SLAM

The traditional visual SLAM framework has matured considerably over the past few decades. Monocular SLAM was first solved using an extended Kalman filter (EKF) [39], [40].

PTAM [41] is the first keyframe-based multi-thread SLAM system. Keyframe-based methods can do optimization with only a few frames, making it a cost-effective method. After that, almost all the following SLAM framework runs a real-time local tracking thread, which we call frontend, and a slower global consistency mapping thread, which call backend.

According to the way of front-end tracking, SLAM can be divided into direct [42], [43] and indirect [4], [44] systems. Direct methods require feature points to be extracted and matched and tracked by optimizing reprojection error to estimate motion and results. Direct methods directly use pixel intensity in the image to optimize pose and structure by minimizing photometric error. There are also systems that use semi-direct tracking methods such as SVO [2], [45], which extracts FAST features, tracks features using direct methods, and optimizes camera trajectories and 3D structures using reprojection error from any pixel with non-zero intensity gradients from one frame to another.

In the SLAM framework, the backend maintains a global map of points and keyframes. ORB-SLAM is one of the most outstanding indirect method SLAM frameworks in the last decades. The back-end of ORB-SLAM preserves the relationship between all corresponding keyframes and continuously optimizes both map points and keyframes by local bundle adjustment and global bundle adjustment. In recent years, with the promotion of low-cost IMU, VINS has been widely used. A VINS (visual-inertial system) [3], [46], [47] usually consists of a small sliding window as frontend and combined with a lightweight pose-graph-based backend, which will not save the correspondence of keyframes and only optimize the keyframe poses through loop closure. In this work, to better verify our methods, we implement our method both in a full backend of ORB-SLAM3 and a lightweight backend of VINS.

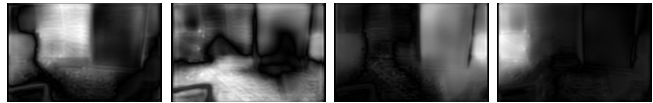
C. Deep Dense Mapping

[10], [11] present end-to-end approaches for addressing the challenge of monocular dense mapping. [12], [13] focus on reconstructing dense meshes from provided images and poses. [15] builds upon the work of [14] by introducing dense reconstruction. However, all these methods require large amounts of computation resources.

In recent years, with the development of depth prediction, many researches have focused on combining depth prediction results with SLAM systems. Sun et al. [32] designed two depth prediction networks, one for predicting relative depths to improve Visual Odometry accuracy, and another for predicting scale-consistent depths for dense mapping. Liu et al. [48] utilize the predicted depth to improve the initialization and map point triangulation. Yang et al. [31] incorporate the outputs of depth prediction networks and pose prediction networks into the DSO [42] to address the issue of scale ambiguity. However, the problem with these methods is that once the depth is predicted by the network will not be optimized anymore. CNN-SLAM [30] predicts depth from a single frame and uses dense depth alignment to generate the 3D dense map. Koestler et al. [49] propose a CVA-MVSNet based on MVSNet [50] to predict depth from several pose-given images, and the depth

will be fused into TSDF. The front-end tracking depends on the updated TSDF, which leads to the low efficiency of the method. Another creative way to continuously optimize the depth in the BA process is variational auto-encoders [36]–[38], [51]. However, these methods are heavy reliance on GPU, limiting the implementation on mobile.

III. BBC-NET

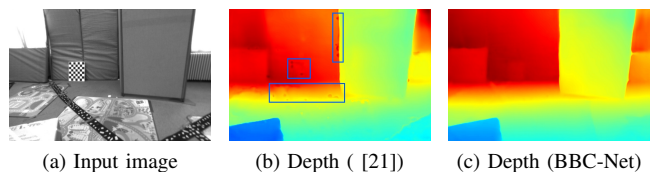


(a) Multi-basis predicted by BBC-Net, scaled with the same factor.



(b) Multi-basis predicted by [21], scaled with the same factor.

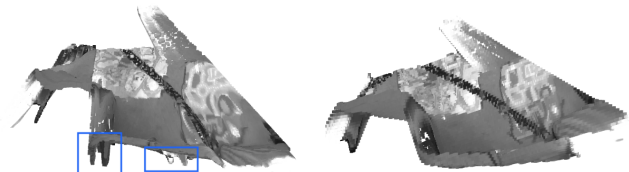
Fig. 3. (a) The depth bases predicted by our network exhibit excellent information distribution, with each base learning the relative depth of a region. (b) The depth bases generated by [21] exhibit obvious imbalance, with typically only one base output containing almost all the information.



(a) Input image

(b) Depth ([21])

(c) Depth (BBC-Net)



(d) Mesh generated by (b)

(e) Mesh generated by (c)

Fig. 4. Outliers are highlighted with blue boxes. Although outliers constitute a small proportion of the predicted depths, they are clearly visible as prominent protrusions in the corresponding 3D mesh.

The main issue with [21] is that the depth bases predicted by [21] suffer from significant imbalance, which manifests in two aspects: firstly, there are notable imbalance in the information learned by each depth base, with typically only one depth base outputting almost all of the information (as shown in Figure 3); secondly, there is also an imbalance in the learned information within each individual depth base, with the network overfitting to the input sparse depths, resulting in spots around these sparse depths (Figures 4(b) and (c)). The issues arising from these imbalances are amplified when integrating with SLAM systems. The reason is that the sparse depths generated by SLAM systems (introduced in Sec. V) are often in low accuracy and are likely to be adjusted or even discarded as outliers during subsequent optimization. A straightforward method to address this imbalance issue is to re-predict the depth bases after each optimization. However, it is

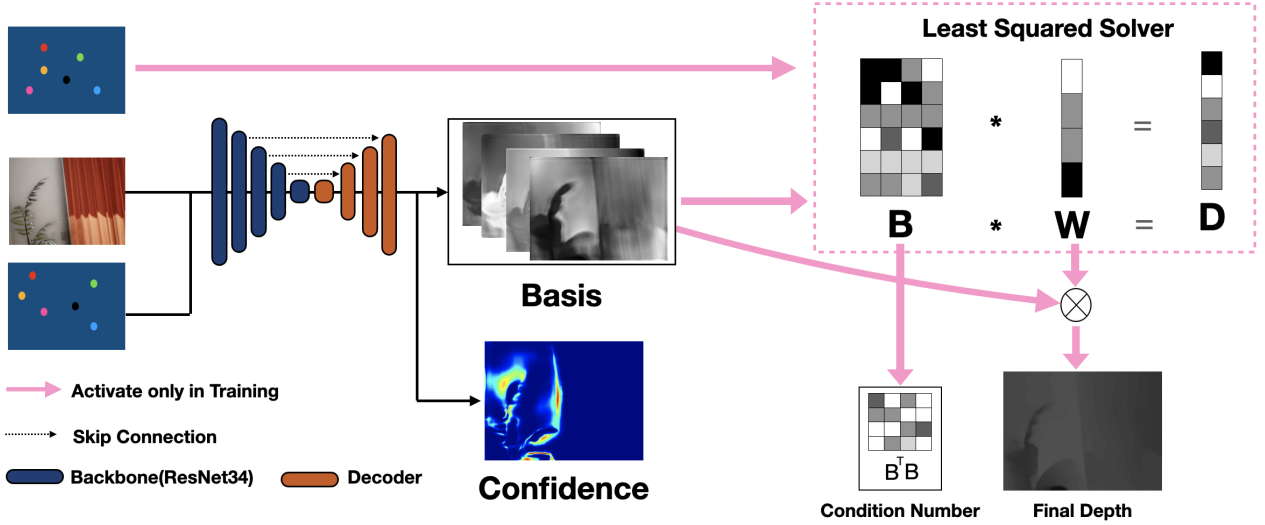


Fig. 5. BBC-Net architecture. The network takes a grayscale image and sparse depth as inputs and outputs a set of depth bases and a confidence map. The pink arrow is activated only in the training process.

evident that this approach is highly computationally expensive and not feasible. In addition to the issue of imbalanced bases, the optimizer in SLAM systems is highly sensitive to depth prediction errors. Therefore, when adding factors to the optimizer, it is crucial to avoid sampling points with significant prediction errors as much as possible.

To overcome the above problems, we propose BBC-Net, a multi-basis network designed to integrate with SLAM systems. As illustrated in Figure 5, BBC-Net consists of two modules: an encode-decoder network and a linear least-squares solver module, similar to the approach presented in [21]. The linear least square module estimates the weight of bases with the generated bases and the input sparse depths during the training process. The inputs to the network include a gray-scale image and sparse depths, and the network produces two branches of output: an N -dimensional vector of bases, with the same resolution as the input, and a corresponding confidence map for the input image. Since [21] do not release their code, we implement their method by ourselves as a baseline and further develop our network based on it. Here, we will only introduce the main improvements we made compared to the baseline, and for more implementation details about baseline and BBC-Net, please refer to [21] and our supplementary materials. In our experiments, the result of [21] were all referring to the baseline versions that we implemented by ourselves.

Compared to [21], our approach makes several important improvements. Firstly, we have incorporated an additional confidence output. Secondly, we have added the bases balance loss and the confidence loss to the training loss function. Lastly, we have enhanced the supervised training process to avoid overfitting on the input sparse depths. Our loss function is defined as follows:

$$L = L_d + w_c L_c + w_b L_b, \quad (1)$$

where L_d is the depth consistency loss, L_c is confidence loss, L_b is bases balance loss, w_c and w_b is the weight of L_c and L_b . In this paper, w_c is set to 2, while w_b is set to 0.1

The depth consistency loss can be simply defined as follows:

$$L_d = \|(D_{gt} - D_{pred})\|. \quad (2)$$

Confidence Loss We aim to assign higher confidence to areas with high accuracy in depth prediction, while penalizing high confidence in regions with significant depth prediction errors. Inspired by [52], we define the confidence loss as follows:

$$L_c = \|(D_{gt} - D_{pred}) \circ C\|_1 + w_0 \left\| \frac{1}{C+1} \right\|_1, \quad (3)$$

where C is the confidence of the predicted depth. $\left\| \frac{1}{C+1} \right\|_1$ is designed to prevent C from approaching to 0. The corresponding weight w_0 is set to 0.1

Bases Balance Loss Basis-fitting methods typically obtain the final depth by a linear combination of the bases.

$$D = \sum_{i=1}^N w_i B_i, \quad (4)$$

where B stands for bases and D stands for final depth. The weights of different bases are usually determined by minimizing the difference between the predicted depth and the depth of the sparse points in the input. That is

$$\arg \min_W \sum_{j=1}^k (S_j - \sum_{i=1}^N (w_i B_i(x_j))), \quad (5)$$

where S stands for the vector of sparse depth, and x stands for the corresponding sparse point. The above optimization problem can be simplified to a linear problem as follows:

$$(B^T B)W = B^T S. \quad (6)$$

The condition number can be defined as follows:

$$cond = \frac{\lambda_{max}(B^T B)}{\lambda_{min}(B^T B)}, \quad (7)$$

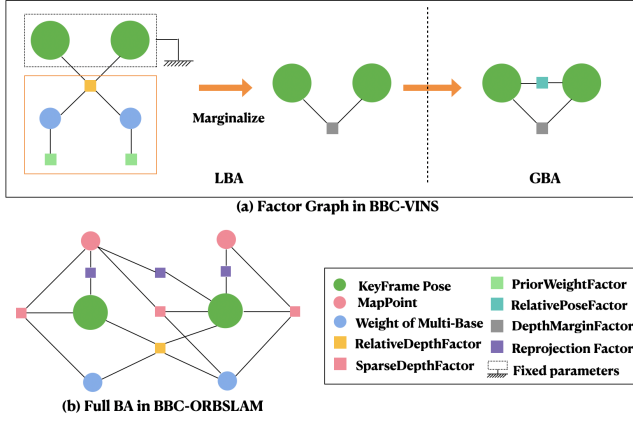


Fig. 6. BA Factor Graph. (a) The factor graph of BBC-VINS. (b) The factor graph of BBC-ORB.

where λ_{max} , λ_{min} is the max and min eigenvalue of the matrix.

When the bases exhibit significant imbalance, the condition number grows large and the problem becomes ill-posed. Consequently, even slight noise in the input sparse depth or the corresponding point of the predicted bases can result in substantial deviations in the weights, leading to erroneous outcomes. Hence, we incorporate the condition number into our loss function to mitigate such effects. This not only eliminates the interference of outlier values during training but also enables us to supervise the depth balance. According to [53], the eigenvalue is differentiable; Therefore the condition number is also differentiable. We design the bases balance loss based on condition number, which is defined as follows:

$$L_b = \log(\lambda_{max}(B^T B)) - \log(\lambda_{min}(B^T B)). \quad (8)$$

Bases Balance Training During the depth prediction process, sparse depth is utilized in two steps: 1) the network combines the input image and sparse depth to predict the depth bases, and 2) the least squares module utilizes the predicted depth bases and sparse depth to solve for the weights of the depth bases. To prevent the network from overfitting to information near the sparse depth and causing an imbalance within the depth bases, we have chosen distinct sparse depth points from pre-extracted FAST corners during the training process for each of the two steps.

IV. DEPTH WEIGHT OPTIMIZATION

In this section, we will present several optimization factors for the weight of depth bases. The factor graph of our system is depicted in Figure 6. For convenience explanation, we pre-defined some notations and symbols here. R_i and t_i is rotation matrix and translation matrix of frame i respectively. w_i is the weight of bases of frame i , the dimension of w_i is $n \times 1$, n is the num of bases. D_i are the depth bases of image i , $D_i(p)$ is bases values in point p at image i , the dimension of $D_i(p)$ is equal to the dimension of weight w_i . X_{w_k} is the position of map point k . π is the projection function to project 3D point to image. Specifically, we define R_z as $(0, 0, 1)^T$.

A. Sparse Depth Factor

The sparse depth factor aligns the final depth with the sparse map points. As map points are observed by multiple keyframes, this factor can provide constraints between multiple keyframes. Specifically, if we fix the pose of the keyframe and the position of map points, the function of this factor is equivalent to that of the least squares method described in [21]. The error can be defined as follows:

$$E_{D_{ik}} = R_z^T (R_i X_{w_k} + t_i) - D_i (\pi (R_i X_{w_k} + t_i))^T w_i. \quad (9)$$

In light of the potential for SLAM to optimize the sparse points used as input for the BBC-Net, we did not employ the least squares solver described in [21] during the online inference process. Instead, after the network predicts the depth bases, we obtain the latest map point coordinates and utilize this sparse depth factor to independently optimize the weight of the depth bases.

B. Relative Depth Weight Factor

When enough overlap exists between frame i and frame j , we will sample points in frame i with a similar point sample method to [42]. For sample point p in frame i , we can get its corresponding depth $D_i^T(X_p)w_i$. Then, we can project this point to frame j as

$$X_{c_j} = R_j (R_i^T (\pi^{-1}(X_p) * D_i^T(X_p)w_i - t_i)) + t_j. \quad (10)$$

So, the relative depth error can be defined as follows:

$$E_{R_{ijp}} = R_z^T X_{c_j} - D_j^T (\pi(X_{c_j})) w_j. \quad (11)$$

While the sparse depth factor can provide constraints between multiple frames, many of the map points used in this factor are corners, which limits its contribution to depth consistency. Its main role is to ensure optimization stability, rather than enhancing depth consistency. Indeed, the relative depth factor remains the most significant contributor to depth global consistency.

C. Prior Weight Factor

The definition of the prior factor is relatively simple. The error of the prior weight factor can be defined as follows:

$$E_{P_i} = \hat{w}_i - w_i, \quad (12)$$

where \hat{w}_i is the result of w_i in last optimization iteration.

Under conditions of insufficient constraints, optimization divergence may occur. In fact, we consider it abnormal for the depth to undergo significant changes before and after optimization. Therefore, adding a prior factor is logical and can improve the robustness of the optimization.

D. Weight Marginalization

Generating a large number of sampling points that are added as observations to the optimizer can significantly reduce its efficiency. To improve the efficiency of the optimizer, we can use marginalization. When the oldest frame slides out of the LBA window, we marginalize the relative depth weight factors and prior weight factors related to the oldest frame and

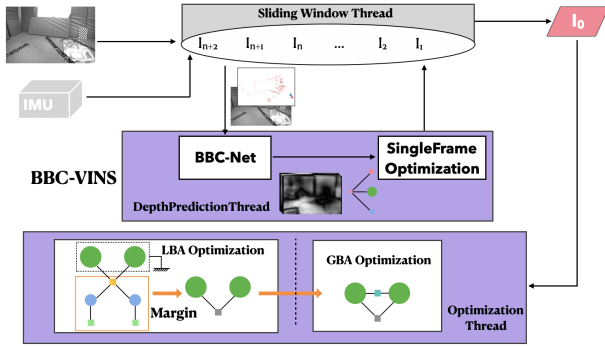


Fig. 7. The architecture of BBC-VINS. In BBC-VINS, we employ a two-stage optimization strategy. In LBA optimization, the camera poses are fixed, and only the weights of the depth bases are optimized. On the other hand, camera poses are optimized in GBA optimization.

save these marginalized information separately. During GBA optimization, this marginalized information can be directly added to the optimizer. Similar to the method in [3], marginalization is achieved through Schur complement. Marginalizing the weights of the depth bases avoids redundant observations and significantly improves the optimizer’s efficiency.

V. SLAM FRAMEWORK

A. BBC-VINS

The architecture of BBC-VINS is shown in Figure 7. In this paper, the BBC-VINS is developed based on our self-implemented VINS system called BVINS. BVINS follows the architecture of [3] but replaces the sliding window optimization with [54]. The length of the sliding window is set to 12. Moreover, BVINS utilizes the KLT optical flow tracker [55], similar to [3], to track the features of FAST corners [56]. To ensure a minimum number of features (100-120) in each image, we supplement the FAST corners in the most recent frame for further visual tracking when the number of successfully tracked features is insufficient. When the frame is still in the sliding window, we will package the image and sparse depth and send it to a separate thread for depth-based inference, which will not affect feature tracking and the efficiency of the sliding window. As previously mentioned, the number of map points that can be tracked in a single frame is usually insufficient. Therefore, we project all points in the sliding window onto the same frame, retain the points still in the viewing range, and use them as sparse depth input to the BBC-Net.

The main modification made in this work involves incorporating depth weight optimization into the backend optimization process. In a traditional pose graph backend, the optimization process only runs when a loop closure is detected. However, in BBC-VINS, the use of relative depth provides additional pose constraints, allowing for pose optimization even in the absence of loop closure. To ensure both efficiency and robustness, we have developed a two-stage optimization strategy involving LBA and GBA. During the LBA stage, only the weights of each depth base are optimized, while during the GBA stage, only the poses are optimized.

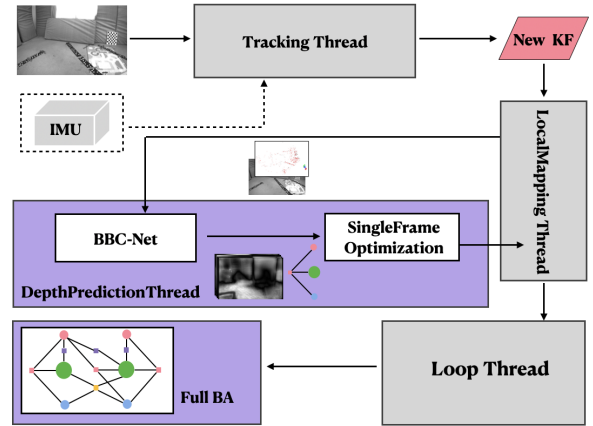


Fig. 8. The architecture of BBC-ORBSLAM. We add the relative depth weight factor and the sparse depth factor to the optimizer, enabling joint optimization of camera poses, map points and the weights of depth bases.

B. BBC-ORBSLAM

The architecture of BBC-ORBSLAM is shown in Figure 8. Original ORB-SLAM3 consists of three threads: Tracking, LocalMapping, and Loop Closure. The keyframes are generated in the LocalMapping thread. Once a keyframe is generated, we will get all local map points from connected keyframes and then project local map points into the image of the current keyframe. After removing the point that cannot project into the image area or with invalid depth, the remaining sparse point combined with the gray image will be sent to BBC-Net, which runs in an independent thread. When a new candidate keyframe comes, the LocalMapping thread will try to get results from the BBC-Net thread. To solve the local inconsistency caused by multi-thread, we will optimize the weight of each base when the result comes back from BBC-Net. Due to the high global accuracy of ORB-SLAM3, we do not need to optimize all the weights at a high frequency. So we add the relative depth factor into Global Bundle Adjustment only.

VI. EXPERIMENTS

In this section, we compare our method with the state-of-the-art dense mapping method, CNN-SLAM [30], CodeMapping [38], Tandem [49], DeepFactors [51] (see VI-A1), GeoRefine [34]. As the relative depth factors will not be activated without global bundle adjustment in BBC-ORBSLAM, the trajectories and depths used in the experiment are the results after dense global bundle adjustment unless otherwise specified. Unlike Tandem [49], our method does not depend on TSDF, so we save the depth and poses and utilize TSDF Fusion alone to generate the mesh. Due to space constraints, we only present part results in the paper. For more implementation details and experimental results, please refer to supplementary materials.

We conduct these comparative experiments on a desktop PC with an Intel i7-8700 CPU (3.2GHz *12) with 24 GB RAM, and use a Nvidia GTX 1060 6GB GPU for inference. In the following experiments, the BBC-Net we use is trained on a subset of ScanNet which is the same as CodeMapping [38]. We use ADAMW optimizer with the default setting. The learning

rate is set to $1e-3$ at the beginning and decreases by 0.2 every 5 epochs totaling 20 epochs. For each frame, we sample 125 fast keypoints as sparse depth. We augment the sparse depth by perturbing 5% of the depth value, and introducing 2 pixels of noise to the point coordinates.

A. Public Dataset

1) *EuRoC*: We evaluate our method on the widely used dataset EuRoC [57]. We only employ the vicon-room sequences for accuracy evaluation, as these sequences offer dense lidar-scanned maps that can serve as ground truth for reconstruction. Within these sequences, we separately evaluate BBC-ORB-SLAM in monocular(V) and monocular-inertial(VI) modes and BBC-VINS. We both evaluate the trajectory and the depth of each frame as [38]. The way we generate the ground truth depth is by rendering the LiDAR data onto each frame, which is the same with [38]. For tandem, we run it with its dataset mode on EuRoC, and get the depth of each frame by rendering the output mesh with its own ground truth pose. The result of CodeVIO, CodeMapping, DeepFactor comes from their paper. The trajectory of DeepFactor comes from [14]. Normally, we use absolute position error to evaluate the accuracy(APE). Specifically, we use Sim(3) alignment to refine the trajectory and the scale of corresponding depths for monocular methods.

The result shows in Table I and Table II. As shown in Table I, our method achieved the best depth accuracy on almost all sequences. We have respectively presented the trajectory accuracy and sparse depth accuracy of OpenVINS, BVINS, ORB-SLAM (V), and ORB-SLAM (VI) as a reference. BBC-VINS and CodeVIO are both developed based on the VINS system. Specifically, BBC-VINS is built upon BVINS, while CodeVIO is based on OpenVINS. It can be observed that the accuracy of our BVINS is comparable to that of OpenVINS, while the accuracy of our BBC-VINS is significantly superior to that of CodeVIO. In addition, our method can optimize both the depth and camera pose in a forward manner, whereas the CodeVIO method may potentially lead to a decrease in trajectory accuracy.

Comparing the results of BBC-ORB-SLAM and CodeMapping, we arrived at the same conclusion. Both methods are developed based on ORB-SLAM3, but our BBC-ORB-SLAM achieved significantly higher depth accuracy than CodeMapping. Although both BBC-ORB-SLAM and GeoRefine [34] are based on ORB-SLAM, GeoRefine has improved the front-end tracking using RAFT-flow, so the improvement in trajectory accuracy is expected. As our method is a flexible plugin, we believe that if it is adapted to a higher-precision SLAM system, such as GeoRefine or Droid-SLAM [14], our final results will be even better.

In addition to quantitative comparisons, we also present in Figure 9 the meshes constructed by our method and the Tandem. Obviously, the mesh reconstructed by Tandem exhibits more noise than our methods. Compared with BBC-ORB-SLAM, the mesh generated by BBC-VINS is a little noisy. The reason is that the BBC-VINS is based on a VINS system, the architecture of which is much light-weight than

TABLE I
EVALUATION ON DEPTH RMSE(M) ON EUROC. THE BEST RESULT IS SHOWN IN BOLD, THE SECOND RESULT IS SHOWN WITH UNDERLINE.

	V101	V102	V103	V201	V202	V203
DeepFactor [51]	1.05	1.03	0.94	1.02	1.53	<u>1.25</u>
Tandem [49]	0.439	0.375	0.858	0.393	0.559	2.82
GeoRef-V [34]	0.241	<u>0.255</u>	0.297	<u>0.258</u>	0.208	0.231
BBC-ORB-V	<u>0.255</u>	0.163	<u>0.325</u>	0.255	<u>0.355</u>	-
GeoRef-VI [34]	0.241	0.251	0.278	0.258	<u>0.312</u>	0.220
CodeMap [38]	0.381	0.369	0.407	0.428	0.655	0.952
BBC-ORB-VI	<u>0.211</u>	0.155	0.169	<u>0.243</u>	0.326	0.198
BBC-VINS	0.186	<u>0.164</u>	<u>0.176</u>	0.241	0.244	<u>0.209</u>

ORB-SLAM3. The point clouds generated by BBC-VINS are noisier than the point clouds generated by BBC-ORB-SLAM.

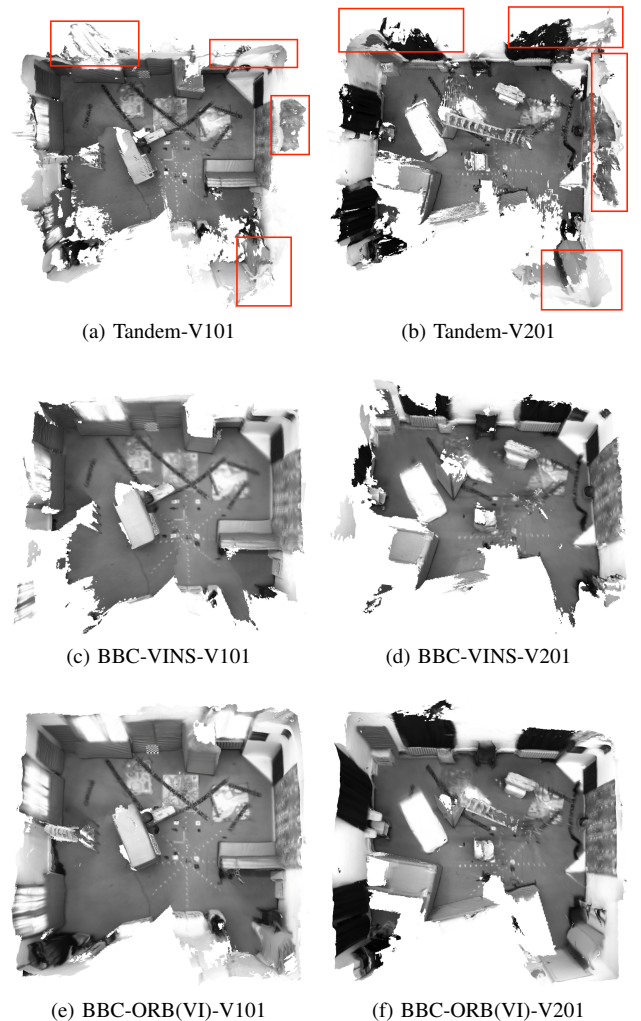


Fig. 9. 3D Models generated by different methods in EuRoC. The red box highlights the portion of the reconstructed mesh with significant errors.

2) *ICL-NUIM & TUM*: We further evaluate our method on both ICL-NUIM [58] and TUM [59] dataset. ICL-NUIM is a synthetic indoor dataset consisting of RGB images and ground truth depths. TUM-RGBD is another well-known dataset mainly for benchmarking the performance of RGB-D SLAM. Due to the lack of available IMU data provided by ICL and TUM, we were unable to validate the BBC-VINS on

TABLE II

EVALUATION ON TRAJECTORY ON EUROC WITH APE(M). THE BEST RESULT IS SHOWN IN BOLD, THE SECOND RESULT IS SHOWN WITH UNDERLINED

	V101	V102	V103	V201	V202	V203
DeepFactor [51]	1.520	0.680	0.900	0.880	1.910	1.020
Tandem [49]	0.100	0.185	0.187	0.106	0.101	0.602
GeoRef-V [34]	0.032	0.010	0.022	<u>0.019</u>	0.011	0.025
BBC-ORB-V	0.035	0.012	0.076	0.016	0.036	-
CodeVIO [37]	0.056	0.072	<u>0.069</u>	0.098	<u>0.061</u>	0.286
BBC-VINS	<u>0.039</u>	<u>0.069</u>	0.096	<u>0.043</u>	0.108	0.147
BBC-ORB-VI	0.033	0.011	0.013	0.018	0.013	0.018
BVINS	0.042	0.072	0.107	0.045	0.113	0.154
OpenVINS [47]	0.056	0.072	0.069	0.098	0.061	0.286
ORB-V	0.035	0.012	0.076	0.016	0.036	-
ORB-VI	0.033	0.011	0.013	0.018	0.013	0.019

these datasets.

We executed BBC-ORBSLAM on both datasets using both RGB and RGBD modes, respectively. To simplify the explanation, we will refer to the RGB mode of BBC-ORBSLAM as BBC-ORB-V, and the RGBD mode as BBC-ORB-VD. It should be noted that when running BBC-ORB-VD, similar to [38], we only used depth information for tracking, while relying on the 3D points generated by SLAM itself for depth prediction and optimization.

Table III and Table IV present our results on the ICL and TUM datasets, respectively. The results of Tandem are not included in Table IV, since it was not evaluated on TUM. Our BBC-ORB-VD achieved the best results across all sequences. The performance of our BBC-ORB-V was hindered on certain sequences of the ICL dataset due to the presence of textureless regions, which pose a significant challenge for monocular SLAM systems. The tracking accuracy of ORBSLAM on these sequences is not high, which adversely affects the performance of BBC-ORB-V. Figure 10 indicates that for texture-rich sequence, BBC-ORB-V can achieve comparable results to BBC-ORB-VD. Figure 13 demonstrates that, for both BBC-ORB-V and BBC-ORB-VD, GBA optimization can help improve depth consistency and enhance the final mesh.

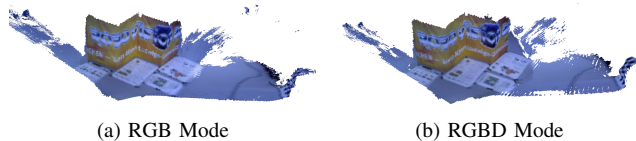


Fig. 10. (a) The mesh generated by BBC-ORB-V. (b) The mesh generated by BBC-ORB-VD.

B. Ablation Study

To intuitively evaluate the role of each module in our system, we performed some ablation experiments. For the sake of clarity, we will use simplified symbols to represent each optimization item. We will use **B** for running with balanced bases, **C** for running with confidence, and **full** for running with balanced base, confidence, and BA optimization, **M** for using marginalization in optimization.

As shown in Table V and Table VI, the incorporation of each of our strategies has led to an improvement in either

TABLE III

EVALUATION OF THE PERCENTAGE OF CORRECT PIXELS δ_1 AS IN [49] ON ICL-NUIM DATASETS. [49] WAS TRAINED ON BOTH SCANNET AND REPLICA DATASETS. THE ASTERISK (*) REPRESENTS THE RESULT WITH TANDEM TRAINED ON SCANNET. OUR MODEL WAS TRAINED ON SCANNET.

	CNN	DF	Tandem	Tandem	Ours	Ours
	- [30]	- [51]	- [49]*	- [49]	-V	-VD
office0	19.41	30.17	52.34	84.04	79.52	84.39
office1	29.15	20.16	61.83	91.18	64.70	96.54
livingroom0	12.84	20.44	86.42	97.00	95.73	97.62
livingroom1	13.03	20.86	71.35	90.62	73.27	95.13

TABLE IV

EVALUATION OF DEPTH ACCURACY ON TUM DATASETS.(SEQ1: FR3 LONG OFFICE HOUSEHOLD; SEQ2: FR3 NOSTRUCTURE TEXTURE NEAR WITHLOOP; SEQ3:FR3 STRUCTURE TEXTURE FAR)

		CNN	DF	GeoRef	GeoRef	Ours	Ours
		[30]	[51]	[34]-V	[34]-VD	-V	-VD
seq1	δ_1	12.48	29.33	-	-	81.23	95.40
	RMSE	-	-	-	-	0.253	0.132
seq2	δ_1	24.08	16.92	-	-	92.90	99.55
	RMSE	-	-	-	-	0.057	0.027
seq3	δ_1	27.40	51.85	-	-	88.25	99.05
	RMSE	-	-	0.317	0.290	0.303	0.064

TABLE V

EVALUATION OF BBC-VINS ON EUROC. *D* STAND FOR DEPTH ERROR, *T* FOR TRAJECTORY ERROR, AND *Sp* FOR SPARSE DEPTH. DEPTH ACCURACY IS MEASURED BY RMSE(M), WHILE TRAJECTORY BY APE(M).

		<i>Sp</i>	[21]	+B	+B,C	+full	+full,M
V101	<i>D</i>	0.511	0.367	0.334	0.200	0.186	0.185
	<i>T</i>	0.042	0.042	0.042	0.042	0.039	0.040
V102	<i>D</i>	0.489	0.359	0.334	0.176	0.164	0.165
	<i>T</i>	0.072	0.072	0.072	0.072	0.069	0.071
V103	<i>D</i>	0.579	0.383	0.363	0.189	0.176	0.173
	<i>T</i>	0.107	0.107	0.107	0.107	0.096	0.098
V201	<i>D</i>	0.486	0.451	0.430	0.256	0.241	0.240
	<i>T</i>	0.045	0.045	0.045	0.045	0.043	0.044
V202	<i>D</i>	0.756	0.624	0.587	0.254	0.244	0.247
	<i>T</i>	0.113	0.113	0.113	0.113	0.108	0.108
V203	<i>D</i>	0.681	0.534	0.495	0.224	0.209	0.209
	<i>T</i>	0.154	0.154	0.154	0.154	0.147	0.151

TABLE VI

EVALUATION OF BBC-ORB(VI) ON EUROC. THE BEST RESULT IS SHOWN IN BOLD.

		<i>Sp</i>	[21]	+B	+B,C	+full
V101	<i>D</i>	0.494	0.379	0.332	0.215	0.212
	<i>T</i>	0.033	0.033	0.033	0.033	0.033
V102	<i>D</i>	0.235	0.264	0.227	0.155	0.155
	<i>T</i>	0.011	0.011	0.011	0.011	0.011
V103	<i>D</i>	0.443	0.268	0.269	0.190	0.169
	<i>T</i>	0.013	0.013	0.013	0.013	0.013
V201	<i>D</i>	0.443	0.396	0.387	0.245	0.244
	<i>T</i>	0.018	0.018	0.018	0.018	0.018
V202	<i>D</i>	0.760	0.582	0.540	0.329	0.327
	<i>T</i>	0.013	0.013	0.013	0.013	0.013
V203	<i>D</i>	0.651	0.338	0.334	0.206	0.198
	<i>T</i>	0.019	0.019	0.019	0.019	0.018

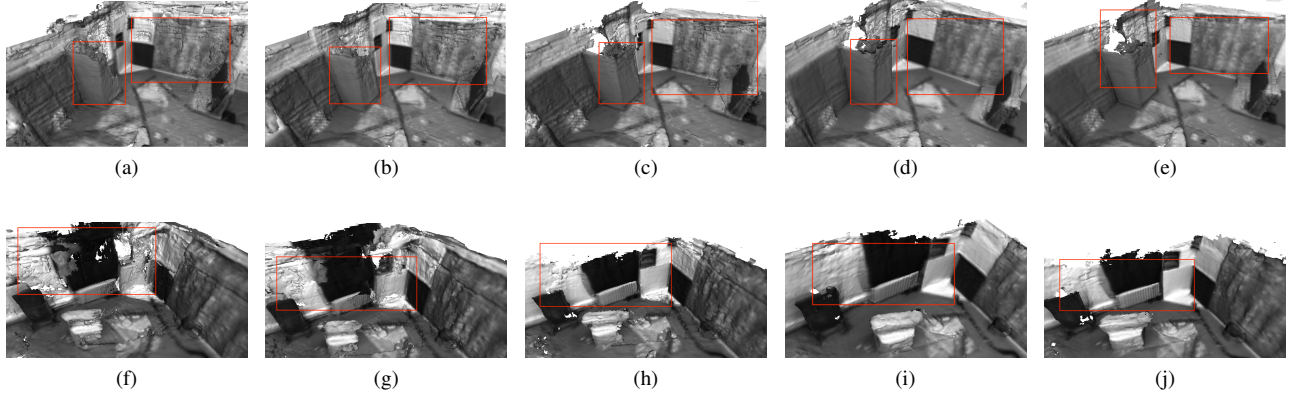


Fig. 11. Meshes generated with BBC-VINS in V102 and V201. The first row corresponds to V102, the second row corresponds to V201. (a) & (f) are the results of [21]. (b) & (g) are the results of $+B$. (c) & (h) are the results of $+B, C$. (d) & (i) are the results of $+full, M$. (e) & (j) are the results of $+full$.

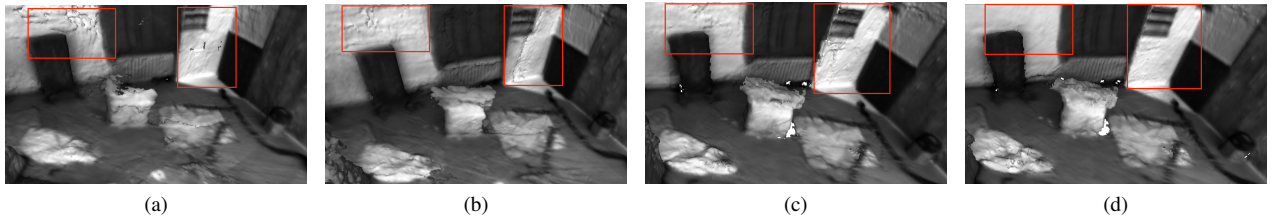


Fig. 12. Meshes generated with BBC-ORB-VI in V203. (a) The result of [21]. (b) The result of $+B$. (c) The result of $+B, C$. (d) The result of $+full$.

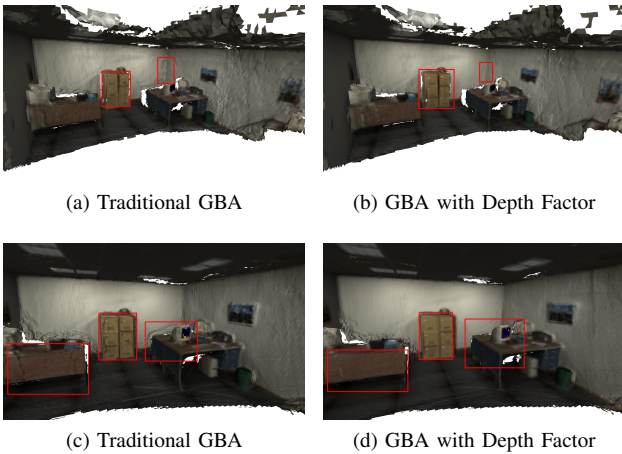


Fig. 13. Mesh generated by BBC-ORB-V in ICL-NUIM. The result of the first row uses RGB input, and the result of the second row uses RGBD input.

trajectory or depth accuracy. Comparing the columns for the baseline ([21]) and $+full$ in the table, it can be observed that our final depth accuracy has been improved by 50% to 100% relative to the [21]. Comparing the columns for $+B, C$ and $+full$, it can be seen that incorporating the weights of depth bases in the optimization can simultaneously improve both depth and trajectory. The improvement in trajectory accuracy is primarily evident in the BBC-VINS system. The reason why BBC-ORB-SLAM has difficulty optimizing the pose is that the ORB-SLAM backend already maintains sufficient observations to ensure trajectory accuracy. The depth factors we designed in Sec. IV are challenging to provide additional constraints

for the keyframe poses. Comparing the column baseline to the ones with $+B$ and $+B, C$, we can conclude that improvements in bases balance and the utilization of confidence can enhance the depth accuracy. From a purely numerical perspective, it is expected that the improvement brought by base balance is not as significant as the improvement brought by confidence. Utilizing confidence information can directly eliminate outliers. Therefore, in terms of numerical indicators, it has the most significant impact on improving depth accuracy. As shown in Figure 4, the work of [21] will cause abnormal depth spots in the predicted depth. These abnormal depths correspond to abnormal protrusions in the reconstructed mesh, while using balanced bases will not. However, since these abnormal depth points account for a very small proportion, they cannot be well reflected numerically. Comparing the $+full$ column and $+full, M$ column, we can observe that marginalization results in little loss in accuracy. On the contrary, it can significantly improve efficiency, which will be discussed later.

In addition to conducting statistical analysis on numerical accuracy, we also visualized the improvements in mesh smoothness brought by the incorporation of each module in Figure 11 and Figure 12. The enhancement of mesh smoothness indicates an improvement in the consistency of trajectories or depth. From Figure 11 and Figure 12, it can be observed that directly incorporating the [21] into the SLAM process generates a mesh with a significant amount of noise. With the improvement of depth-based balance, the mesh becomes smoother. By utilizing confidence measures, large noisy areas are significantly reduced. Moreover, after the BA optimization, the problem of uneven mesh is almost entirely

TABLE VII
MEAN TIME COSTS OF EACH STEP FOR PER FRAME ON AN IPHONE 12 PRO.

	BBC-Net	LBA	LBA (+M)	GBA	GBA (+M)
Time (ms)	20	84	84	7254	4129

resolved. The improvements on the mesh are consistent with the numerical analysis presented in Table V and Table VI.

C. Runtime Measurement

We conducted a time consumption analysis of BBC-VINS on iPhone 12 pro. The inference framework we use is CoreML¹. The average runtime of each module is presented in Table VII. In Table VII, the statistical GBA time corresponds to the optimization time for an average of 58 keyframes. The network uses images with a resolution of 640x480. The depth prediction and LBA optimization are performed in separate threads. Considering the sparsity of keyframes, our method is capable of achieving real-time performance on mobile devices. Although GBA takes longer, it is usually only called when the system is about to quit. Therefore, the time cost of GBA is acceptable as it does not affect the real-time experience. Moreover, Table VII shows that our Marginalization strategy is highly effective, resulting in a 43% speed improvement for GBA. It is worth mentioning that our LBA window size is 8, while CodeMapping uses a window size of 4. And even on a PC, CodeMapping can only achieve a processing rate of 1Hz.

D. Online Demo on a Mobile Phone

To showcase the performance of the proposed method, we have developed an application on mobile. The application takes RGB image stream and IMU measurements obtained from the device as the input and applies BBC-VINS to estimate the poses and depths. Subsequently, the predicted depth of each keyframe is fused into a global TSDF model using the tracked 6DoF pose in a separate fusion thread. Meanwhile, the fused TSDF volume is raycasted by the viewing pose on the frontend, providing users with a real-time preview of the reconstructed mesh. For more details, please refer to the supplementary video. Our fusion method is based on an online incremental mesh generation method Mobile3DRecon [60]. To solve the out-of-memory problem of large-dimension TSDF fusion on mobile platforms, we also refer to the adaptive voxel resizing strategy in [61]. The optimized depths from BA will be re-fused into the TSDF model.

VII. CONCLUSION

In this paper, we propose BBC-Net, an effective depth completion network specifically designed for coupling with the SLAM framework. BBC-Net improves the accuracy of depth completion by addressing the issue of imbalanced bases and adding an additional confidence output. By utilizing the multi-basis depths and confidence, we incorporate the weight of each base into the optimization of the SLAM framework. We have designed multiple factors to optimize the weight of

depth bases, which can be flexibly combined based on the actual scenario. Moreover, our method possesses exceptional portability, allowing seamless integration with a wide range of traditional SLAM systems. The experiment shows that our approach outperforms the state-of-the-art on multiple datasets. Additionally, our method demonstrates high efficiency, making it particularly suitable for real-time dense SLAM. We have also successfully adapted our method for mobile devices and verified its performance.

REFERENCES

- [1] Carlos Campos, Richard Elvira, Juan J Gómez Rodríguez, José MM Montiel, and Juan D Tardós. ORB-SLAM3: An accurate open-source library for visual, visual-inertial, and multimap slam. *IEEE Transactions on Robotics*, 37(6):1874–1890, 2021.
- [2] Christian Forster, Matia Pizzoli, and Davide Scaramuzza. SVO: Fast semi-direct monocular visual odometry. In *IEEE international conference on robotics and automation*, pages 15–22, 2014.
- [3] Tong Qin, Peiliang Li, and Shaojie Shen. VINS-Mono: A robust and versatile monocular visual-inertial state estimator. *IEEE Transactions on Robotics*, 34(4):1004–1020, 2018.
- [4] Haomin Liu, Guofeng Zhang, and Hujun Bao. Robust keyframe-based monocular slam for augmented reality. In *IEEE International Symposium on Mixed and Augmented Reality*, pages 1–10, 2016.
- [5] Jon Zubizarreta, Iker Aguinaga, and Jose Maria Martinez Montiel. Direct sparse mapping. *IEEE Transactions on Robotics*, 36(4):1363–1370, 2020.
- [6] Shahram Izadi, David Kim, Otmar Hilliges, David Molyneaux, Richard Newcombe, Pushmeet Kohli, Jamie Shotton, Steve Hodges, Dustin Freeman, Andrew Davison, et al. KinectFusion: real-time 3d reconstruction and interaction using a moving depth camera. In *Proceedings of the 24th annual ACM symposium on User interface software and technology*, pages 559–568, 2011.
- [7] Thomas Whelan, Stefan Leutenegger, Renato Salas-Moreno, Ben Glocker, and Andrew Davison. *ElasticFusion: Dense slam without a pose graph*. Robotics: Science and Systems, 2015.
- [8] Erik Bylow, Jürgen Sturm, Christian Kerl, Fredrik Kahl, and Daniel Cremers. Real-time camera tracking and 3d reconstruction using signed distance functions. In *Robotics: Science and Systems*, volume 2, page 2, 2013.
- [9] Thomas Schops, Torsten Sattler, and Marc Pollefeys. Bad SLAM: Bundle adjusted direct rgb-d slam. In *Proceedings of the IEEE/CVF Conference on Computer Vision and Pattern Recognition*, pages 134–144, 2019.
- [10] Zak Murez, Tarence van As, James Bartolozzi, Ayan Sinha, Vijay Badrinarayanan, and Andrew Rabinovich. Atlas: End-to-end 3d scene reconstruction from posed images. In *European conference on computer vision*, pages 414–431, 2020.
- [11] Chengzhou Tang and Ping Tan. BA-Net: Dense bundle adjustment network. *arXiv preprint arXiv:1806.04807*, 2018.
- [12] Jiaming Sun, Yiming Xie, Linghao Chen, Xiaowei Zhou, and Hujun Bao. NeuralRecon: Real-time coherent 3d reconstruction from monocular video. In *Proceedings of the IEEE/CVF Conference on Computer Vision and Pattern Recognition*, pages 15598–15607, 2021.
- [13] Zihan Zhu, Songyou Peng, Viktor Larsson, Weiwei Xu, Hujun Bao, Zhaopeng Cui, Martin R Oswald, and Marc Pollefeys. Nice-SLAM: Neural implicit scalable encoding for slam. In *Proceedings of the IEEE/CVF Conference on Computer Vision and Pattern Recognition*, pages 12786–12796, 2022.
- [14] Zachary Teed and Jia Deng. Droid-SLAM: Deep visual slam for monocular, stereo, and rgb-d cameras. *Advances in Neural Information Processing Systems*, 34:16558–16569, 2021.
- [15] Antoni Rosinol, John J Leonard, and Luca Carlone. Probabilistic volumetric fusion for dense monocular slam. In *Proceedings of the IEEE/CVF Winter Conference on Applications of Computer Vision*, pages 3097–3105, 2023.
- [16] Doyeon Kim, Woonghyun Ga, Pyunghwan Ahn, Donggyu Joo, Sehwan Chun, and Junmo Kim. Global-local path networks for monocular depth estimation with vertical cutdepth. *arXiv preprint arXiv:2201.07436*, 2022.
- [17] René Ranfil, Katrin Lasinger, David Hafner, Konrad Schindler, and Vladlen Koltun. Towards robust monocular depth estimation: Mixing datasets for zero-shot cross-dataset transfer. *IEEE Transactions on Pattern Analysis and Machine Intelligence*, 44(3), 2022.

¹<https://developer.apple.com/documentation/coreml/>

- [18] Fangchang Ma and Sertac Karaman. Sparse-to-dense: Depth prediction from sparse depth samples and a single image. In *IEEE international conference on robotics and automation*, pages 4796–4803, 2018.
- [19] Frederik Warburg, Daniel Hernandez-Juarez, Juan Tarrio, Alexander Vakhitov, Ujwal Bonde, and Pablo F Alcantarilla. Self-supervised depth completion for active stereo. *IEEE Robotics and Automation Letters*, 7(2):3475–3482, 2022.
- [20] Youmin Zhang, Xianda Guo, Matteo Poggi, Zheng Zhu, Guan Huang, and Stefano Mattoccia. Completionformer: Depth completion with convolutions and vision transformers. In *Proceedings of the IEEE/CVF Conference on Computer Vision and Pattern Recognition*, pages 18527–18536, 2023.
- [21] Chao Qu, Ty Nguyen, and Camillo Taylor. Depth completion via deep basis fitting. In *Proceedings of the IEEE/CVF Winter Conference on Applications of Computer Vision*, pages 71–80, 2020.
- [22] Maximilian Jaritz, Raoul De Charette, Emilie Wirbel, Xavier Perrotton, and Fawzi Nashashibi. Sparse and dense data with cnns: Depth completion and semantic segmentation. In *International Conference on 3D Vision*, pages 52–60, 2018.
- [23] Zhiqiang Yan, Kun Wang, Xiang Li, Zhenyu Zhang, Jun Li, and Jian Yang. RIGNet: Repetitive image guided network for depth completion. In *European Conference on Computer Vision*, pages 214–230, 2022.
- [24] Frederik Warburg, Michael Ramamonjisoa, and Manuel López-Antequera. SparseFormer: Attention-based depth completion network. *arXiv preprint arXiv:2206.04557*, 2022.
- [25] Xinjing Cheng, Peng Wang, and Ruigang Yang. Learning depth with convolutional spatial propagation network. *IEEE transactions on pattern analysis and machine intelligence*, 42(10):2361–2379, 2019.
- [26] Alex Wong and Stefano Soatto. Unsupervised depth completion with calibrated backprojection layers. In *Proceedings of the IEEE/CVF International Conference on Computer Vision*, pages 12747–12756, 2021.
- [27] Xinjing Cheng, Peng Wang, Chenye Guan, and Ruigang Yang. CSPN++: Learning context and resource aware convolutional spatial propagation networks for depth completion. In *Proceedings of the AAAI Conference on Artificial Intelligence*, volume 34, pages 10615–10622, 2020.
- [28] Mu Hu, Shuling Wang, Bin Li, Shiyu Ning, Li Fan, and Xiaojin Gong. PENet: Towards precise and efficient image guided depth completion. In *IEEE International Conference on Robotics and Automation*, pages 13656–13662, 2021.
- [29] Jinsun Park, Kyungdon Joo, Zhe Hu, Chi-Kuei Liu, and In So Kweon. Non-local spatial propagation network for depth completion. In *European Conference on Computer Vision*, pages 120–136, 2020.
- [30] Keisuke Tateno, Federico Tombari, Iro Laina, and Nassir Navab. CNN-SLAM: Real-time dense monocular slam with learned depth prediction. In *Proceedings of the IEEE conference on computer vision and pattern recognition*, pages 6243–6252, 2017.
- [31] Nan Yang, Lukas von Stumberg, Rui Wang, and Daniel Cremers. D3VO: Deep depth, deep pose and deep uncertainty for monocular visual odometry. In *Proceedings of the IEEE/CVF Conference on Computer Vision and Pattern Recognition*, pages 1281–1292, 2020.
- [32] Libo Sun, Wei Yin, Enze Xie, Zhengrong Li, Changming Sun, and Chunhua Shen. Improving monocular visual odometry using learned depth. *arXiv preprint arXiv:2204.01268*, 2022.
- [33] Feihu Yan, Jiawei Wen, Zhaoxin Li, and Zhong Zhou. Monocular dense slam with consistent deep depth prediction. In *Computer Graphics International Conference*, pages 113–124, 2021.
- [34] Pan Ji, Qingan Yan, Yuxin Ma, and Yi Xu. GeoRefine: Self-supervised online depth refinement for accurate dense mapping. In *European Conference on Computer Vision*, pages 360–377, 2022.
- [35] Zachary Teed and Jia Deng. Raft: Recurrent all-pairs field transforms for optical flow. In *European Conference on Computer Vision*, pages 402–419, 2020.
- [36] Michael Bloesch, Jan Czarnowski, Ronald Clark, Stefan Leutenegger, and Andrew J Davison. CodeSLAM—learning a compact, optimisable representation for dense visual slam. In *Proceedings of the IEEE conference on computer vision and pattern recognition*, pages 2560–2568, 2018.
- [37] Xingxing Zuo, Nathaniel Merrill, Wei Li, Yong Liu, Marc Pollefeys, and Guoquan Huang. CodeVIO: Visual-inertial odometry with learned optimizable dense depth. In *IEEE International Conference on Robotics and Automation*, pages 14382–14388, 2021.
- [38] Hidenobu Matsuki, Raluca Scona, Jan Czarnowski, and Andrew J Davison. CodeMapping: Real-time dense mapping for sparse slam using compact scene representations. *IEEE Robotics and Automation Letters*, 6(4):7105–7112, 2021.
- [39] Andrew J Davison. Real-time simultaneous localisation and mapping with a single camera. In *Computer Vision, IEEE International Conference on*, volume 3, pages 1403–1403. IEEE Computer Society, 2003.
- [40] Andrew J Davison, Ian D Reid, Nicholas D Molton, and Olivier Stasse. MonoSLAM: Real-time single camera slam. *IEEE transactions on pattern analysis and machine intelligence*, 29(6):1052–1067, 2007.
- [41] Georg Klein and David Murray. Parallel tracking and mapping for small ar workspaces. In *IEEE and ACM international symposium on mixed and augmented reality*, pages 225–234, 2007.
- [42] Jakob Engel, Vladlen Koltun, and Daniel Cremers. Direct sparse odometry. *IEEE transactions on pattern analysis and machine intelligence*, 40(3):611–625, 2017.
- [43] Jakob Engel, Thomas Schöps, and Daniel Cremers. LSD-SLAM: Large-scale direct monocular slam. In *European conference on computer vision*, pages 834–849, 2014.
- [44] Raul Mur-Artal, Jose Maria Martinez Montiel, and Juan D Tardos. ORB-SLAM: a versatile and accurate monocular slam system. *IEEE transactions on robotics*, 31(5):1147–1163, 2015.
- [45] Christian Forster, Zichao Zhang, Michael Gassner, Manuel Werlberger, and Davide Scaramuzza. SVO: Semidirect visual odometry for monocular and multicamera systems. *IEEE Transactions on Robotics*, 33(2):249–265, 2016.
- [46] Anastasios I Mourikis and Stergios I Roumeliotis. A multi-state constraint kalman filter for vision-aided inertial navigation. In *Proceedings IEEE international conference on robotics and automation*, pages 3565–3572, 2007.
- [47] Patrick Geneva, Kevin Eickenhoff, Woosik Lee, Yulin Yang, and Guoquan Huang. OpenVINS: A research platform for visual-inertial estimation. In *Proc. of the IEEE International Conference on Robotics and Automation*, Paris, France, 2020.
- [48] Sheng Liu, Xiaohan Nie, and Raffay Hamid. Depth-guided sparse structure-from-motion for movies and tv shows. In *Proceedings of the IEEE/CVF Conference on Computer Vision and Pattern Recognition*, pages 15980–15989, 2022.
- [49] Lukas Koestler, Nan Yang, Niclas Zeller, and Daniel Cremers. Tandem: Tracking and dense mapping in real-time using deep multi-view stereo. In *Conference on Robot Learning*, pages 34–45, 2022.
- [50] Yao Yao, Zixin Luo, Shiwei Li, Tian Fang, and Long Quan. MVSNet: Depth inference for unstructured multi-view stereo. In *Proceedings of the European conference on computer vision*, pages 767–783, 2018.
- [51] Jan Czarnowski, Tristan Laidlow, Ronald Clark, and Andrew J Davison. DeepFactors: Real-time probabilistic dense monocular slam. *IEEE Robotics and Automation Letters*, 5(2):721–728, 2020.
- [52] Hyesong Choi, Hunsang Lee, Sunok Kim, Sunok Kim, Seungryong Kim, Kwanghoon Sohn, and Dongbo Min. Adaptive confidence thresholding for monocular depth estimation. In *Proceedings of the IEEE/CVF International Conference on Computer Vision*, pages 12808–12818, 2021.
- [53] Christoph Boeddeker, Patrick Hanebrink, Lukas Drude, Jahn Heymann, and Reinhold Haeb-Umbach. On the computation of complex-valued gradients with application to statistically optimum beamforming. *arXiv preprint arXiv:1701.00392*, 2017.
- [54] Kejian Wu, Ahmed M Ahmed, Georgios A Georgiou, and Stergios I Roumeliotis. A square root inverse filter for efficient vision-aided inertial navigation on mobile devices. In *Robotics: Science and Systems*, volume 2. Rome, Italy, 2015.
- [55] Jianbo Shi and Tomasi. Good features to track. In *Proceedings of IEEE Conference on Computer Vision and Pattern Recognition*, pages 593–600, 1994.
- [56] Edward Rosten and Tom Drummond. Machine learning for high-speed corner detection. In *European Conference on Computer Vision*, volume 1, pages 430–443, May 2006.
- [57] Michael Burri, Janosch Nikolic, Pascal Gohl, Thomas Schneider, Joern Rehder, Sammy Omari, Markus W Achtelik, and Roland Siegwart. The euroc micro aerial vehicle datasets. *The International Journal of Robotics Research*, 35(10):1157–1163, 2016.
- [58] Ankur Handa, Thomas Whelan, John McDonald, and Andrew J Davison. A benchmark for rgb-d visual odometry, 3d reconstruction and slam. In *IEEE international conference on Robotics and automation*, pages 1524–1531, 2014.
- [59] Jürgen Sturm, Nikolas Engelhard, Felix Endres, Wolfram Burgard, and Daniel Cremers. A benchmark for the evaluation of rgb-d slam systems. In *IEEE/RSJ international conference on intelligent robots and systems*, pages 573–580, 2012.
- [60] Xingbin Yang, Liyang Zhou, Hanqing Jiang, Zhongliang Tang, Yuanbo Wang, Hujun Bao, and Guofeng Zhang. Mobile3DRecon: real-time monocular 3d reconstruction on a mobile phone. *IEEE Transactions on Visualization and Computer Graphics*, 26(12):3446–3456, 2020.

- [61] X. Xiang, H. Jiang, G. Zhang, Y. Yu, C. Li, X. Yang, D. Chen, and H. Bao, "Mobile3dscanner: An online 3d scanner for high-quality object reconstruction with a mobile device," *IEEE Transactions on Visualization and Computer Graphics*, vol. 27, no. 11, pp. 4245–4255, 2021.